Hindawi Publishing Corporation
Science and Technology of Nuclear Installations
Volume 2012, Article ID 298452, 8 pages
doi:10.1155/2012/298452

Research Article

Experimental Characterisation of the Interfacial Structure during Counter-Current Flow Limitation in a Model of the Hot Leg of a PWR

Christophe Vallée,[1] Toshifumi Nariai,[2] Takashi Futatsugi,[2] Akio Tomiyama,[2] Dirk Lucas,[1] and Michio Murase[3]

[1] *Institute of Safety Research, Helmholtz-Zentrum Dresden-Rossendorf (HZDR), 01314 Dresden, Germany*
[2] *Graduate School of Engineering, Kobe University, Nada-ku, Kobe-shi, Hyogo 657-8501, Japan*
[3] *Institute of Nuclear Technology, Institute of Nuclear Safety System, Inc. (INSS), Mihama-cho, Mikata-gun, Fukui 919-1205, Japan*

Correspondence should be addressed to Christophe Vallée, c.vallee@hzdr.de

Received 27 November 2011; Accepted 3 February 2012

Academic Editor: Deendarlianto

In order to investigate the two-phase flow behaviour during counter-current flow limitation in the hot leg of a pressurised water reactor, dedicated experiments were performed in a scaled down model of *Kobe University*. The experiments were performed with air and water at atmospheric pressure and room temperature. At high flow rates, CCFL occurs and the discharge of water to the reactor pressure vessel simulator is limited by the formation of slugs carrying liquid back to the steam generator. The structure of the interface was observed from the side of the channel test section using a high-speed video camera. An algorithm was developed to recognise the stratified interface in the camera frames after background subtraction. This method allows extracting the water level at any position in the image as well as performing further statistical treatments. The evolution of the interfacial structure along the horizontal part of the hot leg is shown by the visualisation of the probability distribution of the water level and analysed in function of the liquid and gas flow rates. The data achieved are useful for the analysis of the flow conditions as well as for the validation of modelling approaches like computational fluid dynamics.

1. Introduction

In the event of hypothetical accident scenarios in a pressurised water reactor (PWR), emergency strategies have to be mapped out, in order to guarantee the reliable removal of the decay heat from the reactor core, also in case of component breakdown. Therefore, the primary circuit is designed to favour a natural circulation which allows to release the heat to the secondary circuit over the steam generators (SGs). One essential passive heat removal mechanism is the reflux cooling mode. In the reflux condenser mode, the water level in the reactor pressure vessel (RPV) is already reduced to the level of the hot leg nozzle or even below, consequently, only steam flows to the steam generator. The steam coming from the RPV condenses in the vertical U-tubes of the steam generator and, in each half of the steam generator, the condensate flows down the tube in which it has been formed. Therefore, about one half of the condensate flows as usual over the pump to the downcomer, whereas the other part flows over the hot leg back to the upper plenum. In the hot leg, the condensate has to flow in counter current to the steam.

However, the stratified counter-current flow of condensate and steam is only stable for a certain range of flow rates. In fact, if the steam flow increases too much, the condensate is clogged in the hot leg. This is the onset of the counter-current flow limitation (CCFL): the liquid is carried over by the steam and partially entrained in opposite direction to the steam generator. As a consequence, the hot leg and steam generator are flooded, which decreases the water level in the RPV and reduces the core cooling. In case of an additional increase of the steam flow, the condensate is completely blocked and the reflux cooling mode ends. In this situation the cooling of the reactor core from the hot leg is impossible,

but may be continued by coolant drained through the cold leg to the downcomer.

The reflux condenser cooling mode can appear for instance during a small break loss of coolant accident (LOCA) or because of a loss of residual heat removal (RHR) system during midloop operation at plant outage after its shutdown. For the validation and optimisation of accident management strategies, such transient scenarios are reproduced in dedicated facilities or rather simulated. The use of one-dimensional system codes, which are principally based on empirical correlations, is a common practice. The implemented correlations are adapted to reflect the macroscopic flow characteristics and were extensively validated in the past; consequently, they can be used for safety analyses. However, the correlations do not allow to predict the flow conditions from first principles, and therefore, present limitations. In particular for the flow situations dominated by 3D effects, a computational fluid dynamics (CFDs) approach is required to evaluate the local behaviour in detail. These simulation methods are not yet mature and have to be validated before they can be applied to nuclear reactor safety. Therefore, dedicated experimental data is needed with high resolution in space and time.

To support the theoretical model development and the validation of CFD codes, air/water counter-current flow experiments were performed in a scaled down model of the hot leg of a PWR built at Kobe University. The present study investigates the structure of the interface observed from the side of the channel test section using a high-speed video camera. After some image scaling evaluations, an algorithm developed to recognise the stratified interface in the camera frames after background subtraction will be presented. Finally, the evolution of the water level along the hot leg will be analysed in function of the liquid and gas flow rates with help of statistical treatments showing the global structure of the interface.

2. Previous Investigations of Counter-Current Flow Limitation in PWR Hot Legs

The first detailed investigations on counter-current flow limitation in a hot leg typical geometry (i.e., a horizontal conduit connected to a riser) date back to the late seventies. Richter et al. [1] performed air/water experiments in a scaled down model of the hot leg of a PWR. The test section was made of acrylic glass in order to allow visual observation of the two-phase flow. They proposed to correlate the obtained flooding data with the nondimensional superficial velocity introduced by Wallis [2] in 1969 for vertical counter-current flows in pipes. In 1980, Krolewski [3] established the experimental flooding characteristic of five different hot leg geometries with air and water. She shows that the characteristic of the CCFL depends significantly on the angle of the riser as well as on the inlet and outlet geometry.

Later on, Ohnuki [4] performed counter-current flow limitation experiments in a horizontal pipe connected to an inclined riser with air/water and saturated steam/water both under atmospheric pressure conditions. From his results, Ohnuki concluded that the flooding characteristics are independent from the fluid combination. Furthermore, he varied the most important geometrical aspects of the hot leg: the conduit diameter, the length of the straight pipes, and the angle of the riser. As a result of his investigations, Ohnuki proposed an empirical correlation to predict the onset of flooding by using the Wallis parameter, in which the y-intercept constant is a function of the length to diameter ratio of the horizontal pipe as well as of the length of the inclined riser.

Furthermore, steam/water CCFL experiments under increased pressure conditions were performed in the Upper Plenum Test Facility (UPTF), which simulates the primary circuit of a PWR at full scale. The experiments related by Weiss and Hertlein [5] simulate the reflux condenser mode after a small break LOCA. These were conducted at pressures of 3 and 15 bar and saturation conditions. A comparison of the results with the correlations of Richter et al. and Ohnuki confirmed that the Wallis parameter allows a proper geometrical scaling of the effects of counter-current flow limitation.

More recently, Kim and No [6] have merged in one database the experimental results obtained by eight different research groups, which were published between 1986 and 1999. The database includes cold air/water as well as steam/water experiments. By the regression through a total of 356 data points, Kim and No proposed a flooding correlation as function of the length to diameter ratio of the horizontal part of the hot leg. The prediction error of the correlation was evaluated against the considered database to 8.7%.

This brief review of the literature shows that previous investigations cover many aspects of the CCFL in hot leg typical geometries. However, the goal of most of the previous experiments was the development and validation of one-dimensional system codes. Therefore, the available data mainly focuses on macroscopic effects, which do not allow a detailed validation of the CFD codes. In fact, for comparison with CFD calculations, dedicated experimental data are needed with high resolution in space and time, for instance by the application of optical measuring techniques.

Such "CFD grade" experiments were recently performed at *Helmholtz-Zentrum Dresden-Rossendorf* (cf. Vallée et al. [7]). The structure of the two-phase flow was observed with a high-speed video camera in a model of the hot leg with rectangular cross-section at reactor typical boundary conditions (saturated steam/water at up to 50 bar and 264°C). However, the large scale of the test facility as well as the harsh boundary conditions unfortunately do not allow to observe the complete hot leg. Therefore, the complementary test facilities available at Kobe University were used for additional air/water experiments. The first results obtained in Kobe were reported by Minami et al. [8], including flow pattern maps, hysteresis effects between flooding and deflooding as well as the CCFL characteristics. Furthermore, Nariai et al. [9] investigated the influence of the fluid properties on the CCFL characteristics, varying the liquid phase viscosity with glycerol/water solutions.

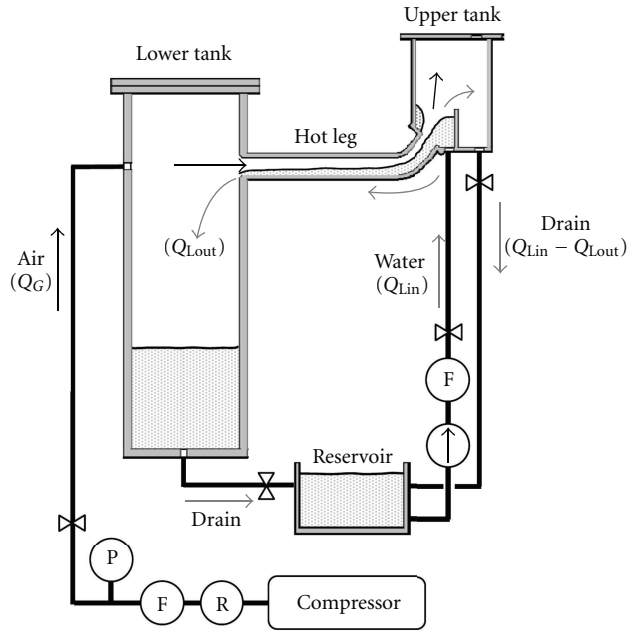

P: pressure guage, F: flow meter, R: regulator

(a) scheme of the experimental setup

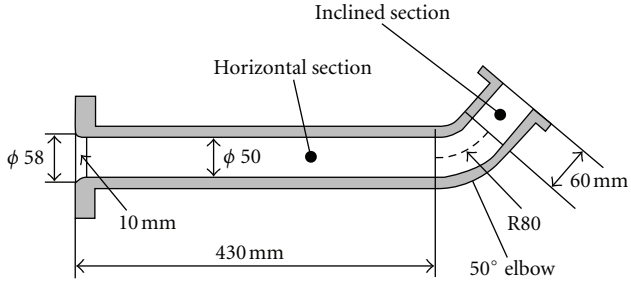

(b) hot leg test section

Figure 1: Hot leg test facility of Kobe University.

3. Experimental Setup and Procedure

Figure 1 shows a schematic of the experimental setup. It consists of the upper tank corresponding to the inlet plenum of a steam generator (SG), of the hot leg test section, and of the lower tank simulating the reactor pressure vessel (RPV). Furthermore, the experimental setup includes supply systems for the air and the liquid as well as a water reservoir. Details of the hot leg test section are shown in Figure 1(b). The hot leg consists of a horizontal section, a 50° elbow and an inclined section. It is scaled at 1 : 15 compared to the original nuclear power plant, corresponding to an inner diameter D of 50 mm. The dimensions of the separators are $L \times H \times W = 300 \times 1000 \times 100$ mm and $200 \times 160 \times 300$ mm for the lower and upper tank, respectively. The hot leg and the separators are made of transparent acrylic resin to allow optical observations.

Air is supplied from an oil-free compressor through a control valve and a flow meter (FLT-N, Flowcell, Ltd.) to the lower tank (cf. Figure 1(a)). The opening for the air is

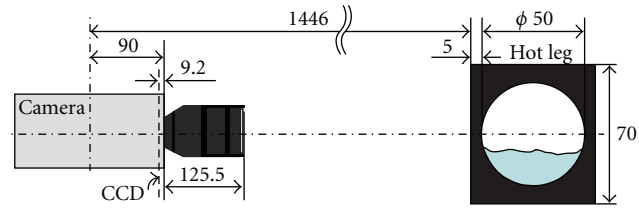

Figure 2: Cross-section of the hot leg pipe and position of the camera.

situated opposite to the one for the hot leg test section. The liquid (tap water) is injected to the bottom of the upper tank by a magnet pump via a flow meter (FLT-N, Flowcell, Ltd.) and flows through the test section into the lower tank. The experiments were performed at room temperature and atmospheric pressure, the air being discharged to the environment from the upper tank. The measuring uncertainties for the inlet superficial water velocity $j_{L,\text{in}}$ and for the superficial gas velocity j_G were estimated with 95% of confidence at ±3.0% and ±2.5%, respectively.

The upper tank is divided into two parts by a 105 mm high weir placed at 110 mm of the left wall (cf. Figure 1(a)). This volume below the weir simulates the volume of the original steam generator inlet plenum. When CCFL occurs in the hot leg, the part of liquid which overflows the weir in the upper tank is drained into the reservoir. This design allows quasistationary counter-current flow limitation experiments. However, the separation area does not simulate the effects of the steam generator itself. In general, the water head in the upper tank does not significantly affect the CCFL characteristics. However, the fluctuation of the water head affects the fluctuation of pressure in the lower tank as well as the gas inlet flow rate into the hot leg. Consequently, this effect influences the CCFL characteristics due to a nonlinear behaviour. For further general information concerning this effect, please refer to the study by Navarro [10].

During the experiments, constant water and air flow rates were injected into the test facility. The air volume flow rate was varied from 0 to 15.7 L/s (corresponding to superficial gas velocities j_G in the pipe of 0 to 8 m/s) and the inlet water flow rate from 0.17 to 0.50 L/s (i.e., $j_{L,\text{in}} = 0.085, \ldots, 0.25$ m/s). The experimental series were started with high air flow rates where CCFL is clearly established in order to avoid hysteresis effects (cf. Minami et al. [8]).

4. Optical Observations

Optical measurements were performed with a high-speed video camera. The flow was filmed from the side of the channel at 300 frames per second. Depending on the fluctuation of the flow structures over time, the recording time was varied between 20 and 30 s, leading to 6000 to 9000 images.

4.1. Image Scaling. As shown in Figure 2, the camera was placed at approximately 1.4 m from the channel. The settings lead to a spatial resolution of the images of about 2.2

pixel/mm (cf. example in Figure 5). In order to evaluate the distortion of the recorded images, the optical path was modelled from the camera objective to the hot leg model. As shown in the cross-sectional view (cf. Figure 2), the test section is not a pipe in a strict sense, it is a rectangular block of acrylic glass drilled in the centre. The result of the simulation is shown in Figure 3 for a half-filled test section and a distance between camera and channel outer wall of 100 mm. This short distance was chosen in order to intensify the optical refraction effects. Refractive indexes of 1.00, 1.333, and 1.49 were assumed for the air, the water, and the acrylic glass, respectively. As shown in Figure 3, the cross-section geometry corresponds to a divergent lens. However, due to the high index difference between air and acrylic glass, the divergence is more important in the empty part of the hot leg, compared to the domain filled with water. Furthermore, a part of the channel cannot be observed because of total reflection on the round acrylic glass interface.

Moreover, the model was used to evaluate the vertical distortion and resolution of the camera observation. Therefore, it was assumed that the bottom of the interface visible on the camera images corresponds to its left border in contact with the acrylic glass. In fact, due to the divergence of the test section, in the lower half of the channel a lower water level can only be observed if the interface is more concave than the inclination of the light path in water. As this does not apply for the upper half, a second optical path was simulated assuming that the bottom of the interface corresponds to the opposite border of the test section (curve "simulation 2" in Figure 4). Furthermore, the model allows to calculate the limit of total reflection from which the interface is visible on the image: 2.8 mm for the water and 8.4 mm for the air from the top or bottom of the pipe ($y = \pm 25$ mm in Figure 3), respectively.

In order to check the model, calibration measurements were performed before the CCFL experiments. Therefore, the test section was filled with a defined stratified water level and recorded with the high-speed video camera. The position of the interface in the camera images was plotted in function of the measured water level and compared with the simulation results in Figure 4. The simulated line was scaled linearly in pixels in function of the position of the top and bottom outer border of the test section (at $y = \pm 35$ mm, cf. Figure 2). As shown in Figure 4, the agreement between calibration measurements and simulation 1 is good, while simulation 2 gives wrong results. Consequently, this modelling shows that the bottom of the interface visible on the camera images corresponds to the left contact point between the channel and the air/water interface.

4.2. Image Processing Method. In order to capture the gas/liquid interface in the camera frames, an image processing algorithm was developed. As the top of the interface is difficult to identify automatically (in particular due to light reflexions on the water surface and to the background illumination differing for full and empty conditions), the current procedure detects its bottom limit. The principle of the capture method is illustrated in Figure 5 and consists in the following steps:

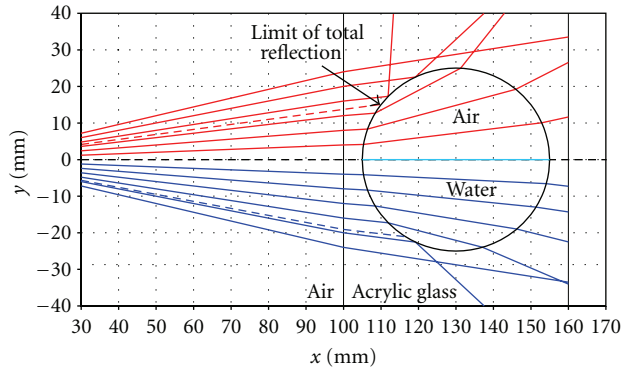

Figure 3: Scheme of the simulated optical path through the hot leg cross-section (distance between camera and channel outer wall: 100 mm).

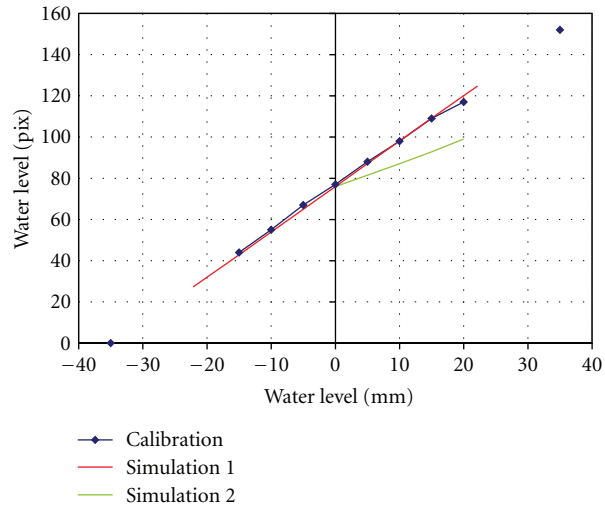

Figure 4: Vertical resolution of the optical observation: comparison between experimental calibration and simulation.

(1) synthesis of a background image (bottom: full channel/top: empty channel, cf. Figure 5(b));

(2) background subtraction (Figure 5(c));

(3) calculation of a vertical gray level gradient over 3 pixels (top and bottom neighbours), cf. Figure 5(d);

(4) searching for the maximum gradient in each vertical line (Figure 5(e));

(5) filtering and detection of the wrong pixels:

  (a) linear interpolation of single outlier with the neighbours (limit = 7 pixels),

  (b) detection of the wrong group of pixels from their distance to the local moving average calculated over 10 neighbours to left and right (distance > 7 pixels);

(6) correction of the wrong group of pixels:

  (a) calculation of the linear interpolation line joining the last well detected pixels;

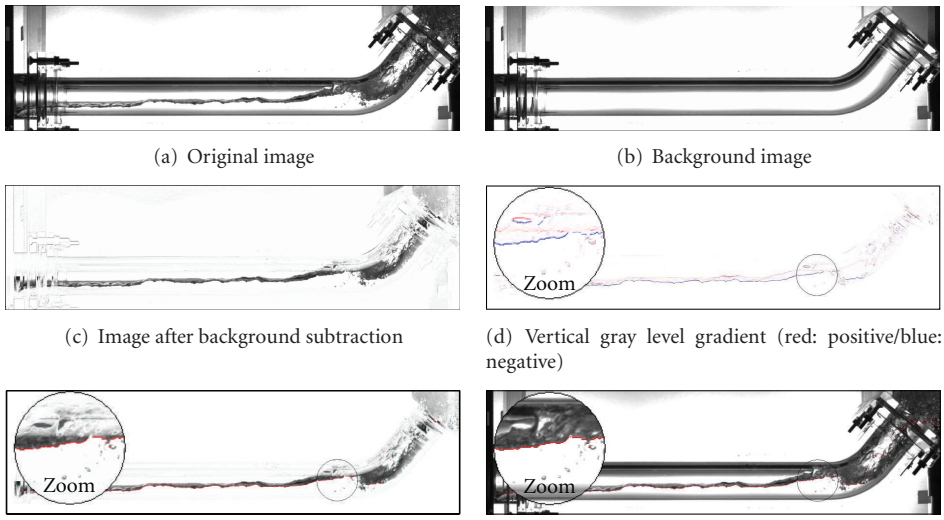

(a) Original image

(b) Background image

(c) Image after background subtraction

(d) Vertical gray level gradient (red: positive/blue: negative)

(e) Points of maximum gradient: good points in red, as incorrect recognised points in blue

(f) Final detected interface (red pixels) over original image

FIGURE 5: Visualisation of the main steps of the image processing (image taken during CCFL at $j_{L,\text{in}} = 0.25$ m/s and $j_G = 4.0$ m/s).

(b) downweighting with a normal distribution weight function the gradient calculated in step (3) in function of the distance to the linear interpolation line;

(c) researching for maximum gradient in the vertical line (Figure 5(f)).

As shown in Figure 5(f), the method gives very good results in the horizontal part of the hot leg. However, due to flanges and seals, the flow in the last part of the test section to the RPV simulator is only partially visible, disturbing the measurement in this region. Furthermore, in the riser to the SG tank, the low contrast between background and interface as well as the annular character of the flow leads to a largely incorrect detection. Consequently, the measurement results will not be analysed in these problematic regions hereafter.

5. Results

5.1. Water Level History. As an example, the experiment chosen to illustrate this section was performed at following boundary conditions:

(i) water flow rate: 0.50 L/s (i.e., $j_{L,\text{in}} = 0.25$ m/s).

(ii) air flow rate: 7.9 L/s (i.e., $j_G = 4.0$ m/s).

The water level in a cross-section as a function of time is obtained from the coordinates of the pixels detected in the high-speed camera images over a complete sequence. As an example, Figure 6 shows the resulting water level history for 7 chosen cross-sections identified by a colour on the picture above. The axial positions are indicated relatively to the inner wall of the lower tank (RPV simulator). Because the images are processed separately, few single outlier were observed in the time plot, which were averaged with the neighbours if the position difference was exceeding 5 pixels.

Along the horizontal part of the hot leg, wavy flow was observed during CCFL and, consequently, the water level presents relatively small fluctuations. The propagation direction of small waves is ambiguous, whereas some larger waves generated close to the bend pass through the hot leg to the lower tank (cf. arrow). In the bended region, the fluctuation of the water level is higher due to the water flow recirculation as well as slug generation, involving bubble formation. Here, the waves propagate in both directions, depending if the wave is high enough to grow unstably to a slug or not.

5.2. Probability Distribution of the Water Level

5.2.1. Calculation and Graphical Representation. As shown in previous section, the interface dynamics depends on the position in the test section. Therefore, a statistical approach is proposed in order to reflect the structure of the interface over time. The probability distribution of the water levels was calculated in each vertical cross-section for the complete measuring time (30.0 s, i.e., 9000 frames). As the image processing algorithm gives one single water level for each axial coordinate, the probability of the water levels measured at the pixel with the coordinates (x, y) is evident to calculate. The obtained probability distribution was represented according to a coloured scale and was superposed to the background picture in Figure 7. This shows relatively thin distributions with high probabilities in the horizontal part of the hot leg, especially close to the RPV simulator. In the direction of the bend, the probability expends due to the generation of larger waves and slugs as mentioned in previous section. The results in the problematic regions of the flange and seals close to RPV simulator as well as in the riser are questionable and should not be analysed. Consequently, these parts were not represented hereafter.

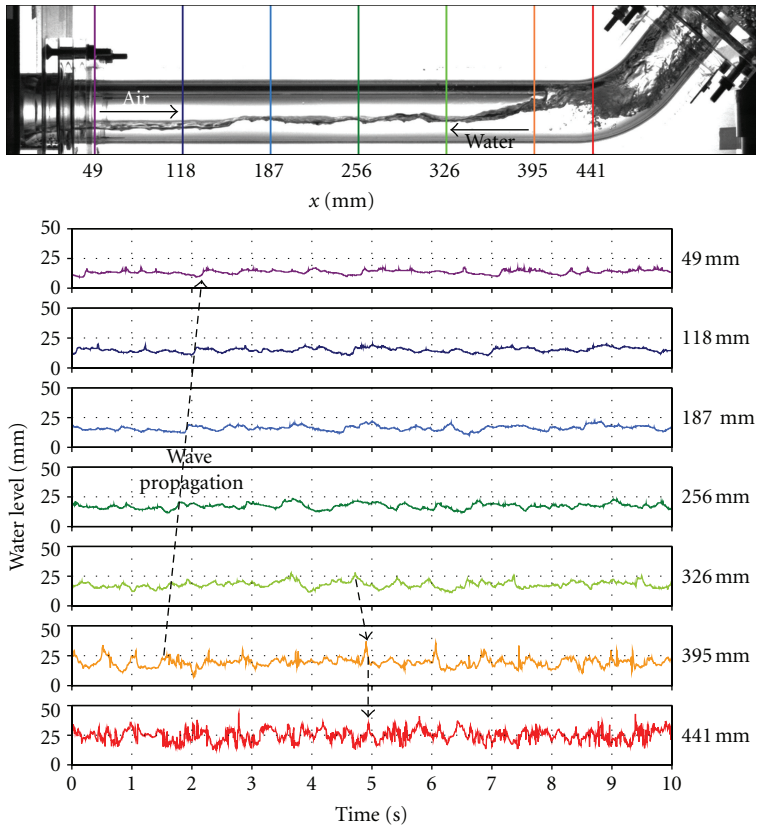

Figure 6: Time-dependent water level in chosen cross-sections during CCFL at $j_{L,\text{in}} = 0.25$ m/s and $j_G = 4.0$ m/s.

Figure 7: Visualisation of the probability distribution of the water level (colours) over the background picture (black and white)—CCFL at $j_{L,\text{in}} = 0.25$ m/s and $j_G = 4.0$ m/s.

5.2.2. Evolution of the Stratified Structure with the Boundary Conditions during CCFL. A series of experiments was performed at a constant injection of water corresponding to a superficial velocity of 0.25 m/s, while the air superficial velocity was varied from 0 to 8.0 m/s. The resulting visualisations of the probability distribution of the water level are shown in Figure 8. Without air flow rate (cf. Figure 8(a)), the water flow in the test section is supercritical (Fr > 1) because of the acceleration occurring down the riser. This explains why the water level increases in downstream direction due to the pressure drop. At air superficial velocities higher or equal to 1.0 m/s, CCFL is reached in the hot leg. According to the structure of the probability distribution, two different flow behaviours were observed.

(i) At low air flow rates (i.e., $1.0 \leq j_G \leq 2.0$ m/s), the probability distribution is broad, indicating a highly fluctuating water level. These large fluctuations are due to the development of large liquid pockets obstructing the complete cross-section and expelled to the steam generator separator by the air flow. These structures originate from large water amounts intruding regularly into the hot leg from the upper tank and correspond to the oscillatory flow pattern described by Minami et al. [8]. This process occurring at relatively long time intervals, the water level in the hot leg decreases drastically in between of two water pockets, explaining the amplitude of the probability distribution.

(ii) At high air flow rate (i.e., $j_G \geq 4.0$ m/s), the water level is low and relatively stable with high probabilities. This is attributed to the frequent development of large waves or small slugs, which do not reach the top of the pipe, transporting the water back to the SG tank more continuously compared to the large liquid pockets.

At $j_G = 8.0$ m/s, the discharge liquid flow to the RPV simulator is null (i.e., zero liquid penetration). The stratified liquid in the horizontal pipe does not reach the lower exit, although it is longer than visible in the images due to the total reflexion effects (cf. Section 4.1). However, compared to previous CCFL conditions, the general structure of the interface is not affected by the zero liquid penetration.

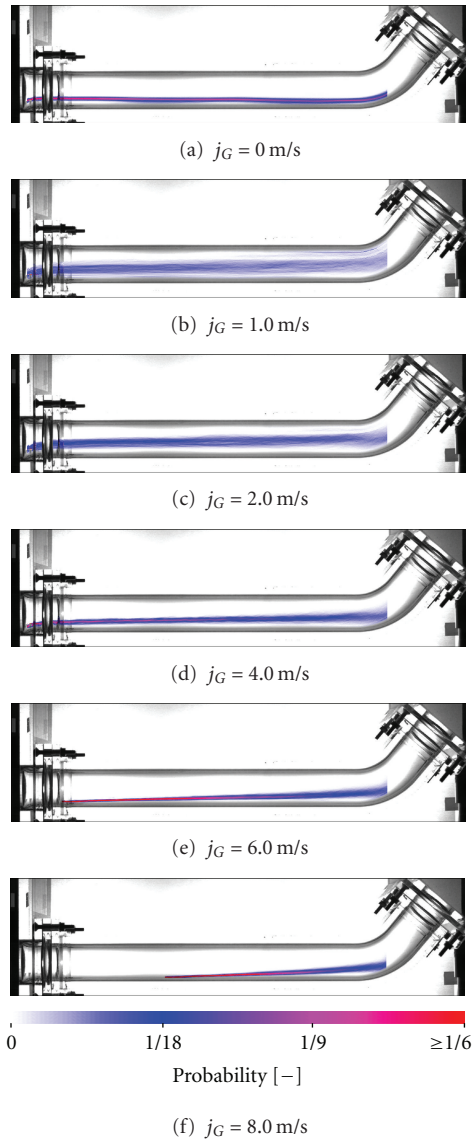

FIGURE 8: Evolution of the probability distribution of the water level in function of the air flow rate for experiments with $j_{L,\text{in}}$ = 0.25 m/s.

Furthermore, series of experiments were performed to check the independency of the interface structure to the inlet water flow rate. As an example, the results obtained at a constant gas superficial velocity of 4.0 m/s and injected water superficial velocities of 0.085 to 0.25 m/s are shown in Figure 9. At these boundary conditions counter-current flow limitation is achieved in the hot leg. As expected, the probability distributions of the water level present no visible dependence on the injected water flow rate.

Moreover, for air superficial velocities higher than 4.0 m/s, the water level in the horizontal section presents an overall linear increase from left to right (cf. Figures 8 and 9). This result supports the assumption made to the water level in a simple CCFL model based on a momentum balance, which was proposed in the literature (Ohnuki et al. [4]).

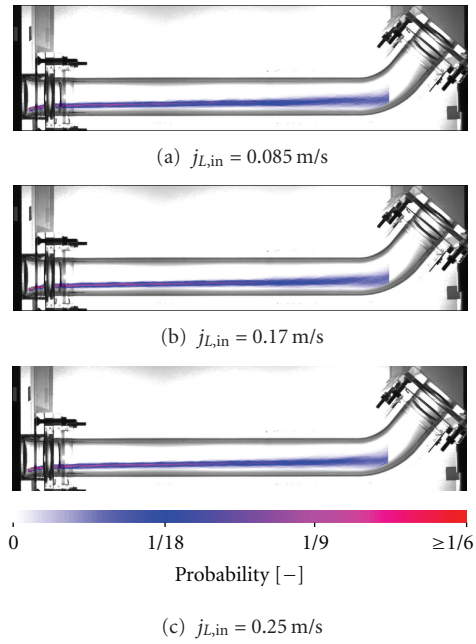

FIGURE 9: Evolution of the probability distribution of the water level in function of the injected water flow rate for experiments with j_G = 4.0 m/s.

6. Summary and Conclusions

In order to investigate the two-phase flow behaviour during counter-current flow limitation in the hot leg of a pressurised water reactor, dedicated experiments were performed in a scaled down model of Kobe University. The structure of the interface was observed from the side of the channel test section using a high-speed video camera. An algorithm was developed to recognise the stratified interface in the camera frames after background subtraction. This method allows extracting the water level at any location of the image as well as further statistical treatments. The evolution of the water level along the horizontal part of the hot leg in function of the liquid and gas flow rates was shown.

It was found that the flow structure during CCFL depends on the flow regime in the hot leg: at low gas velocities large liquid pockets were observed, while at high flow rates the formed slugs are smaller but more frequent. This effect influences the amplitude of the water level fluctuations significantly. Furthermore, the probability distributions of the water level present no visible difference in function of the injected water flow rate. Finally, at high air flow rates, the water level in the horizontal section was found to follow an overall linear trend, as assumed by simple models developed to predict CCFL.

The achieved high-resolution data and especially the visualisation of the probability distribution are of great use for the analysis of the flow conditions as well as for the validation of modelling approaches, in particular computational fluid dynamics (CFDs). Consequently, this new quality of data can help to better understand the processes governing counter-current flow limitation.

Acknowledgments

This work was realised within the frame of a PROMOS Scholarship of the Technische Universität Dresden found by the DAAD (German Academic Exchange Service) and received by the main author. This paper was presented in original form at the 14th International Topical Meeting on Nuclear Reactor Thermalhydraulics (NURETH-14), September 25–30, 2011, Toronto, ON, Canada.

References

[1] H. J. Richter, G. B. Wallis, K. H. Carter, and S. L. Murphy, "Deentrainment and counter¬current air-water flow in a model PWR hot leg," Tech. Rep. NRC-0193-9, U.S. Nuclear Regulatory Commission Report, Hanover, NH, USA, 1978.

[2] G. B. Wallis, *One-Dimensional Two-Phase Flow*, Mc Graw-Hill, New York, NY, USA, 1969.

[3] S. M. Krolewski, *Flooding Limits in a Simulated Nuclear Reactor Hot Leg*, Massachusetts Institute of Technology, Cambridge, Mass, USA, 1980.

[4] A. Ohnuki, "Experimental study of counter-current two-phase flow in horizontal tube connected to inclined riser," *Journal of Nuclear Science and Technology*, vol. 23, no. 3, pp. 219–232, 1986.

[5] P. A. Weiss and R. J. Hertlein, "UPTF test results: first three separate effect tests," *Nuclear Engineering and Design*, vol. 108, no. 1-2, pp. 249–263, 1988.

[6] H. T. Kim and H. C. No, "Assessment of RELAP5/MOD3.2.2γ against flooding database in horizontal-to-inclined pipes," *Annals of Nuclear Energy*, vol. 29, no. 7, pp. 835–850, 2002.

[7] C. Vallée, T. Seidel, D. Lucas et al., "Counter-current flow limitation experiments in a model of the hot leg of a pressurised water reactor—comparison between high pressure steam/water experiments and low pressure air/water experiments," in *Proceedings of the 13th International Topical Meeting on Nuclear Reactor Thermal Hydraulics (NURETH-13)*, Kanazawa, Japan, 2009, Paper no. 13P1107.

[8] N. Minami, D. Nishiwaki, T. Nariai, A. Tomiyama, and M. Murase, "Countercurrent gas-liquid flow in a PWR hot leg under reflux cooling (I) air-water tests for 1/15-scale model of a PWR hot leg," *Journal of Nuclear Science and Technology*, vol. 47, no. 2, pp. 142–148, 2010.

[9] T. Nariai, A. Tomiyama, C. Vallée, D. Lucas, and M. Murase, "Counter-current flow limitation in a scale-down model of a PWR hot leg," in *Proceedings of the 8th International Topical Meeting on Nuclear Thermal-Hydraulics, Operation and Safety (NUTHOS-8)*, Shanghai, China, 2010, Paper no. 8P0109.

[10] M. A. Navarro, "Study of countercurrent flow limitation in a horizontal pipe connected to an inclined one," *Nuclear Engineering and Design*, vol. 235, no. 10–12, pp. 1139–1148, 2005.